

Application of Constrained Multi-Objective Hybrid Quantum Particle Swarm optimization for Improving Performance of an Ironless Permanent Magnet Linear Motor

Wen-Jong Chen*, Wen-Cheng Su and Yin-Liang Yang

Department of Industrial Education and Technology, National Changhua University of Education, No.2, Shi-Da Road, Changhua City, 500, Taiwan

Received: 22 Nov. 2013, Revised: 20 Feb. 2014, Accepted: 21 Feb. 2014

Published online: 1 Nov. 2014

Abstract: This study presents an ironless permanent magnet linear brushless motor (PMLBM) with three objective functions: maximal thrust force, minimal temperature, and minimal volume. Using response surface methodology (RSM), this study presents a mathematical predictive model with constraints using the penalty functions concept for each objective function. The design variables in this study include magnetic width, magnetic height, magnetic pitch, air-gap, coil width, coil height, and coil diameter. This study uses an elitist hybrid quantum behavior particle swarm optimization algorithm with mutation to solve this multi-objective optimization problem (EMO HQPSO). This elitist mechanism with crowding distance sorting improves the number and diversity of the solutions. Results show that the proposed approach is superior to the non-dominated sorting genetic algorithm (NSGA II) and multi-objective particle swarm optimization (MOPSO), respectively, on the 3D graph Pareto-optimal front. Compared to the initial motor, the thrust force increased by 6.27%, the thrust density increased by 14.9%, and the temperature and volume decreased by 14.03% and 6.25% respectively. These results confirm the satisfactory performance of the proposed solutions.

Keywords: QPSO, RSM, Pareto-optimal front, Linear motor

1 Introduction

The permanent magnet linear brushless synchronous motor (PMLBM) has recently become widely used in machine tools and semiconductor devices because it provides high-speed performance, faster response characteristics, high controllability, and high-precision positioning [1]. However, because of the interaction between the edges of the finite length mover and the teeth slotting of the stator in an iron-core PMLBM, the cogging forces distort the thrust force waveform and cause output power variation. Hence, an effective solution is to use ironless PMLBMs, with no cogging force, magnetic flux leakage reduction, iron loss, or attractive force toward the magnets [2]. These PMLBMs can provide stable thrust force and achieve higher efficiency and performance than iron-core PMLBMs. Although ironless PMLBMs have several advantages over iron-core motors and produce a smooth linear motion, they also lead to lower thrust force

and thrust density compared to iron-core motors. Therefore, several researchers have attempted to optimize the design of ironless PMLBMs. Isfahani [3] analyzed magnet dimensions using the genetic algorithm (GA) to improve the thrust force and thrust ripple. Isfahani et al. [4] used the multi-objective GA method further to improve efficiency and power factor for a low-speed single-sided linear induction motor. Taviana et al. [5] analyzed the magnet dimensions that approximate the sine waveform by using the GA for reducing the thrust ripple and air-gap flux density harmonics. Ender and Ahmet [6] presented an analytical method using a hybrid approach of an equivalent magnetic circuit. They used finite-element analysis to minimize the total computational time and determine the best thrust force.

Previous studies have improved the design optimization of the ironless PMLBM. However, because different design objectives must be simultaneously

* Corresponding author e-mail: wjong@cc.ncue.edu.tw

considered to determine the optimal design variables of the ironless PMLBM, the optimization of one objective may conflict with that of another. Thus, there is no single optimal solution, and a compromise between these objectives is required. However, these studies and findings in the literature use formulations from a single-objective optimization algorithm. Thus, these results are unsuitable for most real-world applications because they do not produce the Pareto-optimal front identifying the set of optimal solutions in the feasible region.

The mathematical predictive model used in this study performs the response surface methodology (RSM) to develop the design method of the ironless PMLBM. The central composite design (CCD) from RSM with a second-order model calculates the individual and interactive effects of the ironless PMLBM design variables. The penalty function method based on the constraint of the permeance coefficient first generates the objective function from RSM by solving a constructed unconstrained optimization problem [7]. To achieve faster convergent velocity and reduce the control parameters, a quantum behavior particle swarm optimization (QPSO) algorithm then solves the response surface models by simultaneously considering maximal thrust, minimal temperature, and minimal volume. To avoid premature convergence and local optimal solutions, the QPSO algorithm adopts a GA mutation operator. The proposed approach also adopts an elite-preserving mechanism with crowding distance sorting. The main purpose of this mechanism is to increase the number and diversity of the optimal solutions [8]. Thus, this study uses an elitist multi-objective hybrid quantum behavior particle swarm optimization (EMOHQPSO) algorithm to determine the optimal design variable values of an ironless PMLBM, including the magnet width, magnet height, magnet pitch, air-gap length, coil width, coil height, and wire diameter. Results demonstrate that the proposed approach in this study possesses superior ability to determine the Pareto optimal front, compared to the non-dominated sorting GA (NSGA II) and multi-objective particle swarm optimization (MOPSO). In other words, the EMOHQPSO algorithm achieves good performance in both converging to the true Pareto-optimal front and maintaining a widely distributed set of solutions. Depending on their specific requirements, developers can adequately select the trade-off operation along the true Pareto-optimal front.

2 Structure and topology of ironless PMLBM

2.1 Geometric Structure

The proposed ironless PMLBM contains a mover with a copper winding and a stator with a U-shaped rack base that has an array of alternate-pole permanent magnets mounted on a bilateral of the U-shaped channel. Based on cost and efficiency considerations, most designs adopt a three-phase equilibrium winding with a phase difference

of 120° motor angle [9]. The former windings of a mover manufactured from copper wires are embedded in epoxy material that slides within the U-shaped channel of the stator. Therefore, the characteristics of the windings can affect the magnetic density [10]. For the same current passing through the windings, an increased number of turns increases the strength of the magnetic field and thrust force. However, this also functions as a major heat source of the entire motor. Hence, the area and diameter of the windings of the mover are significant parameters. As the winding coils commutate, they create a magnetic field that interacts with the magnets of the stator to drive the motor to generate linear motion. Therefore, the magnet dimensions and air-gap length between the mover and stator also affect motor performance. In general, a longer air-gap decreases the thrust density and thrust force. However, a smaller air-gap may cause manufacturing difficulties. Therefore, the air-gap size should be properly chosen to satisfy the requirements of design objective and constraints. Therefore, the air-gap size should be properly chosen to satisfy the requirements of design objective and constraints. Figure 1 shows the structure of the ironless PMLBM. The magnet width (w_m), magnet height (h_m), magnet pitch (τ_m), air-gap (δ), coil width (w_c), coil height (h_c) and wire diameter (d_c) are important design parameters, creating trade-off solutions that must simultaneously consider maximal thrust force, minimal temperature, and minimal volume. Table 1 shows the values of the geometrical parameters of the initial motor.

2.2 Permeance Coefficient

The permeance coefficient of a magnet, referred to as the “operating slope”, load line, or B/H [11], is an important parameter for selecting magnetic material and achieving the optimal effect of ironless PMLBM. A magnet with a higher permeance coefficient generally works at a higher operating point with a certain operating slope. Longer magnets have greater permeance coefficients. The shape and dimension of the magnetic body determines the permeance coefficient. Additionally, when the temperature rises, the permanent magnets may become demagnetized [12]. Therefore, the magnet thickness must be large enough to avoid thermal demagnetization. However, the length of the air-gap decreases as the magnet thickness increases, causing manufacturing difficulties. Therefore, the permeance coefficient is a constraint condition in the design problem of the ironless PMLBM. The permeance coefficient is defined as

$$P_c = \frac{h_m}{\delta} \times \frac{1}{C_\phi}, \quad (1)$$

$$C_\phi = A_m/A_a, \quad (2)$$

where h_m is the magnet height, δ is the air-gap length, C_ϕ is the flux concentration factor, $A_a = W_m \times H$ is the surface

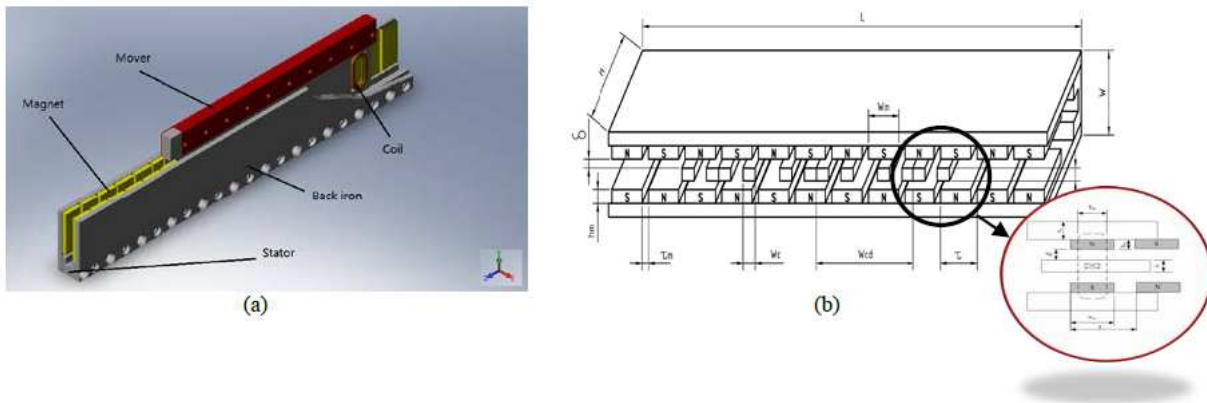


Fig. 1: (a) Illustration of PMLBM (b) Geometrical structure of PMLBM

area of air-gap, $A_m = \tau \times H$ is magnet surface area. For ironless linear motor, the larger the air-gap length is, the lower the P_c of magnet is. In this study, the condition of the P_c is greater than 0.8 [13].

3 Modeling of ironless PMLBM

3.1 Description of Volume

The dimensions of a linear motor affect its mass, dynamic response, inertia, cost, and applied situations. Therefore, the motor volume plays an important role in optimizing the design of the motor body. However, the dimensions of the magnets in the stator affect the retentivity of the linear motor, thereby affecting the thrust force and thrust density. Hence, the volume of the entire motor body must be properly designed to improve motor performance. Let τ , H , h_m , L , δ and h_c be the pole pitch, total height, magnet height, total length, air-gap length and coil height of motor body, respectively. As shown in Fig. 1(b), the volume of the total motor is defined as

$$V = (12\tau)(2h_mL + 2\delta + 2h_c)H. \tag{3}$$

3.2 Thrust and thrust density analysis

Because the forcer windings in the mover are supplied with a current in a direction perpendicular to a magnetic field, an induced thrust force causes the mover to move along the direction perpendicular to the directions of both the current and the magnetic field. The formulation of thrust force generated is generally described as

$$F = N_c I_c B l_c, \tag{4}$$

where I_c is the amount of current flowing through N_c turns of wire, B is magnetic field of flux density in air-gap, l_c

is the length of wound coil in air-gap. The $N_c I_c$, called “ampere turns”, is described as follows [14]:

$$N_c I_c = \sqrt{\frac{P \epsilon A_c}{\rho l_c}}, \tag{5}$$

where P is total power supplied to the coil, ρ is resistivity of the coil, ϵ is the area space factor for the coil, A_c is the coil area. The thrust density is the ratio of generating thrust force at the certain input power and the motor volume. It is one of the most important operational characteristics of the ironless-type linear motor. Thus, the optimal values of the design variables with a higher thrust force and thrust density can improve operating performance. Let V be the volume of the total motor. The thrust density D is defined as follows:

$$D = \frac{F}{V} = \frac{B \left(\frac{P \epsilon A_c l_c}{\rho} \right)^{1/2}}{24H \tau_m (2h_m L + 2\delta + 2h_c)}. \tag{6}$$

3.3 Temperature analysis

Because the mover slides along the U-shaped channel of the stator in ironless-type linear motors, it creates worse heat dissipation heat than iron-core linear-type motors. The operating temperature of the windings in the mover increases with high-speed operation or long working time. Hence, the parts of the motor with various heat coefficients may exhibit the deformation phenomenon. Deformation affects the position precision, operation point of permanent magnets, and dynamic response. To analyze the heat source of the ironless PMLBM, the following formulas consider the heat loss dissipation from the mover:

$$J = \frac{I_c}{A_c}, \tag{7}$$

$$W = M N_c I_c^2 R = M N_c I_c^2 \kappa \frac{2l_c}{A_c}, \tag{8}$$

$$Q = \frac{W}{W_{cH}} = MN_c J_c^2 \kappa \frac{2l_c}{W_{cH} A_c}, \quad (9)$$

where M is the number of winding phase, J is the density of current, W is the copper losses of windings, R is the resistant ratio of each copper wire, Q is heat flow density derived from the surface of the mover, κ is the electrical resistivity of the copper wire.

3.4 Modeling of initial motor

The FEM analysis model of the initial ironless PMLBM calculated by COMSOL software. This model consists of the 12-pole PMs arranged in the U-shaped channel of stator and the three-phase winding coils of the mover. Table 1 shows the dimensions of the initial motor.

4 Response Surface Methodology

Response surface methodology (RSM) consists of a group of mathematical and statistical techniques that can be used to find the relationships between the response and independent variables [15]. The RSM approach is an appropriate approximating model for the true response surface, and can evaluate the design variables for generating the optimization response values. This study uses a second-order prediction equation to model the curvature in the true response function. The CCD of 7-factors and 3-levels selected a starting point as an experimental center position is applied [16]. The second-order response equation was formulated as follows:

$$f = \beta_0 + \sum_{j=1}^m \beta_j x_j + \sum_{j=1}^m \beta_{jj} x_j^2 + \sum_{j=1}^{m-1} \sum_{p=1}^m \beta_{jp} x_j x_p, \quad (10)$$

where x_j and x_p are input variables that influence the response Y ; m is the number of variables; b_0 is the constant term; b_j is the j th interaction coefficient.

5 Constrained EMOHQPSO algorithm

5.1 Constraint-based Multi-Objective Optimization

A multi-objective optimization problem has a number of optimizing objective functions. Many real-world applications involve sets of constraints when considering a multi-objective optimization problem. In this situation, the constrained optimization problem in the search space consists of two types of solutions: feasible and infeasible [17]. A feasible solution is a vector of design variables in which the final solutions satisfy all the constraints, whereas infeasible regions violate at least one constraint. The following formula presents the multi-objective

optimization problem in its general form:

$$\begin{aligned} & \text{Minimize/Maximize } \{Y_1(X), Y_2(X), \dots, Y_q(X)\}, \\ & \text{s.t. } x \in X, \quad g_k \leq 0, \quad k = 1, 2, \dots, n. \end{aligned} \quad (11)$$

where $Y_i : R^m \rightarrow R^l$, $g_k : R^m \rightarrow R^l$ for $j \in J = \{1, 2, 3, \dots, q\}$, q denotes that the number of objective functions to be minimized or maximized, $k \in K = \{1, 2, 3, \dots, n\}$, and $X \in R^m$ is a m -dimension vector: $X = \{x_1, x_2, \dots, x_m\}^T$. Each x_p ($p = 1, \dots, m$) is bounded by lower and upper limits $x_p^L \leq x_p \leq x_p^U$. $g_k(X)$ is known as inequality constraints, respectively. In general, no solution vector X exists that minimizes/maximizes all the q objective functions simultaneously. A feasible solution is called a Pareto optimal set if no other feasible solution is in the search space for which an improvement in any objective does not simultaneously worsen the value of at least one other objective.

5.2 Penalty function

For a constrained optimization problem, an unconstrained form adding a penalty term to the objective function is constructed. Therefore, the unconstrained objective function is the original objective function with constraints plus a penalty term for each constraint. The penalty term consists of constrained functions multiplied by a positive coefficient. This calculation process can remove the infeasible solution in the penalty function method from the population in each iterative algorithm. A penalty method (for minimization problem) is, generally, defined as [18]:

$$\hat{Y}_j(X) = Y_j(X) + \rho \Phi[g_i(X)], \quad (12)$$

$$\Phi[g_i(X)] = \begin{cases} \sum_{i=1}^k [\max(0, g_i(X))]^2, & g_i(X) < 0, \\ 0, & g_i(X) \geq 0. \end{cases} \quad (13)$$

where ρ is the penalty coefficient, $Y_j(X)$ the original j th objective function of the constrained optimization problem in equation (11), $\hat{Y}_j(X)$ is the modified objective function with penalty term, and $\rho \Phi[g_i(X)]$ is the penalty term. For minimization problem, $\rho \Phi[g_i(X)]$ returns zero if no violation occurs; otherwise, it is positive. The penalty function approach determines the solutions of the unconstrained objective function, eventually converging to the solution of the original constrained optimization problem.

5.3 Quantum-behaved particle swarm optimization

Particle swarm optimization (PSO) is a population-based stochastic optimization technique inspired by the social behavior of bird flocking or fish schooling [19]. In traditional PSO with N particles, each particle represents a potential solution to a problem in an m -dimensional space, and its position and velocity at

Table 1: Dimensions of initial motor

Parameter	Symbol	Unit	Value	Parameter	Symbol	Unit	Value
Air-gap	δ	mm	0.6	Winding pitch	I_s	mm	40.0
Coil width	w_c	mm	5.0	Number of turns			122.0
Coil height	h_c	mm	3.8	Motor length along z-axis	h_b	mm	49.0
Number of phases	M		3.0	Thickness of the back iron	w_{cd}	mm	4.0
Pole pitch	τ	mm	15.0	Wire diameter	N_c	mm	0.4
Magnet height	h_m	mm	4.0	Root mean square value	d_w	A	3.4
Magnet width	w_m	mm	12.4	Thrust	P	N	68.6
Magnet pitch	τ_m	mm	2.6	Temperature	T	°C	99.5
Motor length along x-axis	L	mm	18.0	Volume	V	$10^4 mm^3$	40.1
Motor length along y-axis	H	mm	25.0				

iteration t are denoted as $X_i(t)$ and $V_i(t)$. The following equations update the velocity and position of particle i at the $(t + 1)$ th iteration:

$$V_i(t + 1) = \omega V_i(t) + c_1 r_1 (pbest_i - X_i(t)) + c_2 r_2 (gbest - X_i(t)), \quad (14)$$

$$X_i(t + 1) = X_i(t) + V_i(t + 1), \quad (15)$$

$$\omega = \omega_{max} - [(\omega_{max} - \omega_{min}) / (itera_{max})] \times itera, \quad (16)$$

where ω is the dynamic inertia weight factor. Acceleration coefficients c_1 and c_2 are two positive constants, and r_1 and r_2 are two uniformly distributed random numbers within $[0,1]$. The $pbest_i$ (particle’s best solution) is the position for particle i with the best fitness found thus far. The $gbest$ (global best solution) records the best position discovered by the swarm thus far. In equation (14)-(16), the traditional PSO algorithm can prematurely converge and converge slowly later in the search process. To strengthen optimal search abilities and faster convergence speed, this study develops a QPSO to overcome the disadvantages of the PSO algorithm. In the QPSO algorithm, each particle exhibits quantum behavior in the search process. Only the position vector and one control parameter are considered in the entire feasible region. The probability of each particle appearing at time t is only described in the probability density function $|\psi(x,t)|^2$ of the particle’s position. The iteration formulation of each particle’s position is as follows [20]:

$$mbest_i(t) = \sum_{i=1}^N \frac{P_i(t)}{N}, \quad (17)$$

$$p_i(t) = \phi(t) \times pbest_i(t) + (1 - \phi(t)) \times gbest(t), \quad (18)$$

$$x_i(t + 1) = p_i \pm \alpha |mbest_i(t) - x_i(t)| \times \ln(1/u(t)), \quad (19)$$

$$\alpha = (\alpha_{max} - \alpha_{min}) \times \frac{(max_{iter} - t)}{max_{iter}} + \alpha_{min}. \quad (20)$$

where N is the number of all particles, $mbest$ is the Mean Best position (defined as the mean of the best positions of all particles at time t), and the random numbers u and ϕ are distributed uniformly within $[0,1]$ respectively. The contraction-expansion coefficient α , which controls the convergence speed of the algorithm, is the only parameter in the QPSO algorithm. This coefficient has a dynamic value that decreases from α_{max} to α_{min} as the number of iterations increases. The term $p_i(t)$ is the best position of particle i at time t .

5.4 Mutated elitist mechanism QPSO

The QPSO algorithm has simpler evolutionary equation forms and less parameters than PSO, substantially facilitating the control and convergence in the search space. To avoid trapping into the local optimum region in the search process, the QPSO performs a broader searching through the GA mutation operator. The mutation operation only occurs if a randomly generated number in $[0, 1]$ is less than or equal to the given mutation probability. When a mutation is performed, the number of design variables is multiplied by a random value within $[0, 1]$ to determine which variable in each particle should be mutated in the variable space. Let r_3 and r_4 be random numbers in $[0, 1]$. The ceiling function $ceil(\cdot)$ is the smallest integer greater than or equal to “ $r_3 \times m$ ”. The real-valued mutation operators for each updated particle in equation (21) are as follows:

$$x_{i,s}(t + 1)_{mut} = x_{i,s}^L(t + 1) + r_4 \times [x_{i,s}^U(t + 1) - x_{i,s}^L(t + 1)], s = ceil(r_3 \times m). \quad (21)$$

In this study, m is conducted in the space of 7 design variables. “ s ” is the variable sequence position after the mutation for a new particle. Hence, the “ s ” value is an integral value in $[1, 7]$. In order to promote the number and diversity of Pareto-optimal front solutions, an elitist strategy with non-dominated sorting and crowding distance is used for the updated particle. This approach preserves the current best solutions from one generation to the next. The crowding distance of a particle, defined

as the Euclidean distance between its two adjacent neighbors on the same front, can estimate the density of solutions in its front. Let Y_q^{i+1} and Y_q^{i-1} represent the q^{th} objective function of X_{i+1} and X_{i-1} , which are the neighboring particles to the i^{th} particle. Y_q^{max} and Y_q^{min} are the maximal and minimal values of the q^{th} objective in the feasible space. The crowding distance d_i is as follows:

$$d_i = \sum_{j=1}^q \left| \frac{Y_j^{i+1} - Y_j^{i-1}}{Y_j^{max} - Y_j^{min}} \right|. \tag{22}$$

6 Design Optimization Flowchart of EMOHQPSO

The flowchart in Fig. 2 shows the steps of the entire design procedure.

Step 1: Selection of design variables and levels

Consider that the independent design variables in an ironless PMLBM include the magnet width (x_1), magnet height (x_2), magnet pitch (x_3), air-gap (x_4), coil width (x_5), coil height (x_6), and coil diameter (x_7). Their dimensions are the most effective in volume calculation and performance of the motor. Table (2) shows the units, symbols, and coded levels of variables in RSM. Each independent variable has three levels: -1, 0, and +1. Level -1 is the minimum value of the variables. Level 0 is the initial design value of the variables. Level 1 is the maximum value of the variables.

Table 2: Independent design variables and their coded levels

Coded Levels	x_1	x_2	x_3	x_4	x_5	x_6	x_7
-1	10.9	3	2.1	0.45	4.5	3.3	0.35
0	12.4	4	2.6	0.6	5	3.8	0.4
1	13.9	5	3.1	0.75	5.5	4.3	0.45

Step 2: Design of experiments (DOE)

Use the CCD from DOE with a quadratic model. Based on the ranges of each design variable, 152 different combinations of seven variables at three levels were chosen in random order. The optimal levels of the design variables and the interactions of these variables on objective functions were estimated in this step.

Step 3: FEA calculation and creation of response surface predictive model

Use FEA COMSOL software and MINITAB software to find the second-order predictive models for thrust, temperature, and volume. The variable space is

$X = (w_m, h_m, \tau_m, \delta, w_c, h_c, N_c) = (x_1, x_2, x_3, x_4, x_5, x_6, x_7)$. The formulations of the models are as follows:

$$\begin{aligned}
 Y_P = & 65.7096 + 5.416x_1 + 5.414x_2 + 0.9175x_3 \\
 & - 2.5533x_4 + 2.0913x_5 + 3.0562x_6 - 17.571x_7 \\
 & - 0.7885x_1x_1 - 1.6632x_2x_2 - 0.0968x_3x_3 \\
 & + 0.0973x_4x_4 - 0.5135x_5x_5 - 0.4287x_6x_6 \\
 & + 4.4143x_7x_7 + 0.4553x_1x_2 - 0.4502x_1x_3 \\
 & - 0.375x_1x_4 + 0.4472x_1x_5 + 0.4977x_1x_6 \\
 & - 1.4091x_1x_7 + 0.2933x_2x_3 - 0.1066x_2x_4 \\
 & + 0.1495x_2x_5 + 0.4193x_2x_6 - 1.2007x_2x_7 \\
 & - 0.1092x_3x_4 - 0.0383x_3x_5 - 0.0902x_3x_6 \\
 & - 0.2132x_3x_7 + 0.271x_4x_5 + 0.3098x_4x_6 \\
 & + 0.4347x_4x_7 - 2.2097x_5x_6 - 0.3972x_5x_7 \\
 & - 0.5355x_6x_7,
 \end{aligned} \tag{23}$$

$$\begin{aligned}
 Y_T = & 75.3228 - 0.8687x_1 - 2.4205x_2 - 0.827x_3 \\
 & + 0.5687x_4 + 7.9311x_5 + 3.4654x_6 - 53.1869x_7 \\
 & - 0.7885x_1x_1 - 1.6632x_2x_2 - 0.0968x_3x_3 \\
 & + 0.0973x_4x_4 - 0.5135x_5x_5 - 0.4287x_6x_6 \\
 & + 4.4143x_7x_7 + 0.4553x_1x_2 - 0.4502x_1x_3 \\
 & - 0.375x_1x_4 + 0.4472x_1x_5 + 0.4977x_1x_6 \\
 & - 1.4091x_1x_7 + 0.2933x_2x_3 - 0.1066x_2x_4 \\
 & + 0.1495x_2x_5 + 0.4193x_2x_6 - 1.2007x_2x_7 \\
 & - 0.1092x_3x_4 - 0.0383x_3x_5 - 0.0902x_3x_6 \\
 & - 0.2132x_3x_7 + 0.271x_4x_5 + 0.3098x_4x_6 \\
 & + 0.4347x_4x_7 - 2.2097x_5x_6 - 0.3972x_5x_7 \\
 & - 0.5355x_6x_7,
 \end{aligned} \tag{24}$$

$$\begin{aligned}
 Y_V = & 40.131 + 3.7044x_1 + 3.822x_2 + 1.2348x_3 \\
 & + 0.5733x_4 + 0.9555x_6 + 0.3528x_1x_2 + 0.529x_1x_4 \\
 & + 0.0882x_1x_6 + 0.1176x_2x_3 + 0.0176x_3x_4 \\
 & + 0.0294x_3x_6.
 \end{aligned} \tag{25}$$

Step 4: Formulation of optimization

Use equations (23)-(25) to determine the optimizing objective functions for the ironless PMLBM, including maximal thrust $Y_P(X)$, minimal temperature $Y_T(X)$, and minimal volume $Y_V(X)$. To avoid the thermal demagnetization of magnets, the permeance coefficient is set to greater than 0.8. Therefore, the objective functions, constrain conditions, and the variable ranges are as follows:

$$\begin{aligned}
 & \text{Max } Y_P(X) \\
 & \text{Max } Y_T(X) \\
 & \text{Max } Y_V(X)
 \end{aligned} \tag{26}$$

s.t.

$$g_i(X) = P_c = \frac{h_m}{g} \times \frac{1}{\left(\frac{w_m}{w_m + \tau_p}\right)}$$

$$= \frac{x_2}{(2 \times x_4) + x_6} \times \frac{x_1 + x_3}{x_1}$$

$$10.9mm \leq x_1 \leq 13.9mm$$

$$3mm \leq x_2 \leq 5mm$$

$$2.1mm \leq x_3 \leq 3.1mm$$

$$0.45mm \leq x_4 \leq 0.75mm$$

$$4.5mm \leq x_5 \leq 5.5mm$$

$$3.3mm \leq x_6 \leq 4.3mm$$

$$0.35mm \leq x_7 \leq 0.45mm.$$

Step 5: Penalty function method for constrained objective functions

Use equation (26) to determine the constraint condition for the ironless PMLBM design in this study. Equations (28)-(30) show the penalty function method by modifying the objective functions with adding the penalty term $\rho\Phi[g_i(X)]$ to constrain a condition for feasible region violations. The formulations for objective functions are as follows:

$$\Phi[g_i(X)] = \frac{x_2}{(2 \times x_4) + x_6} \times \frac{x_1 + x_3}{x_1} - 0.8 \tag{27}$$

$$\tilde{Y}_P(X) = Y_P(X) - \rho \left[0, \frac{x_2}{(2 \times x_4) + x_6} \times \frac{x_1 + x_3}{x_1} - 0.8 \right]^2 \tag{28}$$

$$\tilde{Y}_T(X) = Y_T(X) + \rho \left[0, \frac{x_2}{(2 \times x_4) + x_6} \times \frac{x_1 + x_3}{x_1} - 0.8 \right]^2 \tag{29}$$

$$\tilde{Y}_V(X) = Y_V(X) + \rho \left[0, \frac{x_2}{(2 \times x_4) + x_6} \times \frac{x_1 + x_3}{x_1} - 0.8 \right]^2 \tag{30}$$

where ρ is set to 20. If the feasible solution X through the duration of the calculations satisfies the constraint condition, then $g(X) = 0$. If not, then $g(X) = 1$. In other words, this infeasible solution can be removed from the population during the next steps of the iteration algorithm.

Step 6: Initialization of swarm positions

Use a uniform distribution number to initialize a population of particles with random positions in the m-dimension search space. The initial combination of the design variables is random. Equation (26) shows the ranges of design variables of each particle between the upper and low limits.

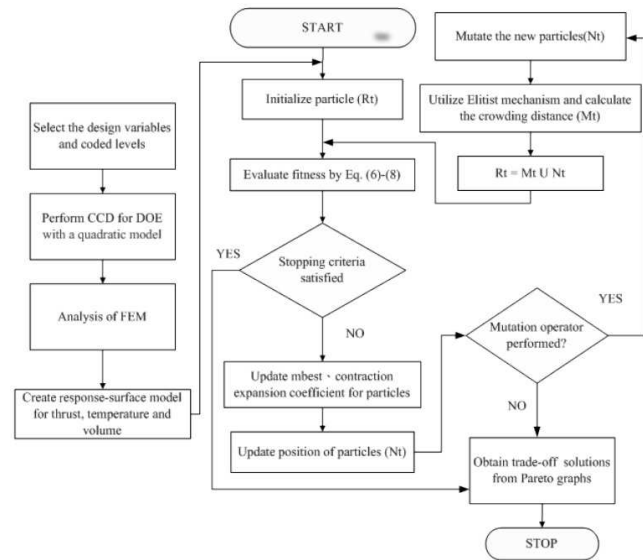


Fig. 2: EMOHPSO Flowchart

Step 7: Evaluate the fitness and check if the stopping criteria is satisfied

Evaluate the fitness value of each particle. Consider the modified objective functions with the penalty term as the fitness function. If the stopping criterion is satisfied, proceed to Step 11. If not, proceed to the next step.

Step 8: Comparison to personal best (pbest) and global best (gbest)

Compare the fitness with each particle's *pbest* and with all swarm's overall previous best values. If the current value of the particle's fitness is better than the *pbest*, then replace the current value with the *pbest* value and replace the current location with the *pbest* location in the m-dimensional space. If the particle's fitness is better than *gbest*, all particles accelerate toward the location of the *gbest*, and the *gbest* must be reset to the current index and value of the particle array.

Step 9: Update the positions of each particle

Using the updating *mbest* and contraction expansion coefficient the new position is determined for each particle using equation (19).

Step 10: Perform the mutation for the updating particle

If the mutation probability is less than or equal to 10% for each updating particle, perform the mutation operation according to equation (21) and proceed to the next step. If not, proceed to Step 12.

Step 11: Perform non-dominated sorting and calculate crowding distance

Step 12: Determine the trade-off solutions

Obtain the 3D graph of the Pareto frontier surface in the objective space from the maximal thrust, minimal temperature, and volume. Find a discrete set of points on the Pareto surface corresponding to high trade-off solutions.

7 Results and discussions

This study presents a way to optimize the performance of ironless PMLBM from RSM with constraints as a constrained multi-objective optimization problem. The optimizing objective functions are maximal thrust force, minimal temperature, and minimal volume, respectively, and the constraint condition is the permeance coefficient. The penalty function method transforms the constrained multi-objective optimization problem into an unconstrained problem that can be solved using the EMOHQPSO algorithm. The initial particles are set at 1000, the contraction expansion coefficient α_{min} and α_{max} as 0.5 and 1.0, respectively. Each particle represents the combination of seven design variables of ironless PMLBM. This study presents results after 500 iterations of the EMOHQPSO performed using Matlab and FEA.

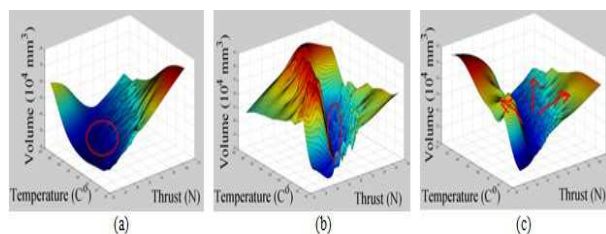


Fig. 3: 3D graph of Pareto optimal solutions of (a) NSGAII (b)MOPSO and (c)EMOHQPSO

Figures 3(a)-3(c) show a 3D graph of Pareto-optimal solutions for the NSGA II, MOPSO, and EMOHQPSO algorithms. Each particle in the EMOHQPSO algorithm appears at any position at a certain probability in the entire feasible region. This is unlike the MOPSO algorithm, which is restricted to searching for particles in a fixed area and a certain track in the search space. In addition, each particle in the EMOHQPSO algorithm has a perfect memory capability, whereas NSGA II rejects worse solutions during the iterations and retains only good solutions. Therefore, in NSGA II, the population includes only a part of the best individuals. In other words, the solutions of the EMOHQPSO algorithm are

closer to the true Pareto-optimal front than those of NSGA II and MOPSO. They are effective in keeping the number and diversity of the swarm. Figures 4(a)-4(c) show projections onto two of the objectives in the 3D Pareto-optimal surface, and present comparisons of the NSGA II, MOPSO, and EMOHQPSO algorithms. The initial linear motor had a thrust force, thrust density, temperature, and volume of 68.6 N, $1.71N/cm^3$, $99^\circ C$ and $40.1 \times 10^4 mm^3$, respectively. Table 3 shows that the set of 14 optimization solutions in EMOHQPSO are excellent solutions along the true Pareto-optimal front. These 14 trade-off solutions simultaneously considering the maximal thrust and thrust density, minimal temperature, and volume for ironless PMLBM are all superior to initial one. Table 3 shows that the thrust force and thrust density increase within 0.72-6.27% and 1.43-14.9 %, respectively. The temperature and volume decrease within 0.14-14.03% and 0.01-6.25%, respectively. According to these 14 trade-off solutions, the solutions of the higher thrust force do not necessarily represent those of the greater thrust density. The temperature and volume can decrease simultaneously in an optimized motor, but the thrust force is not necessarily decreased. Under the same volume, the predictive accuracy of the thrust force and temperature obtained in RSM and FEA are 99.41% and 91.23%, respectively. Therefore, a developer can choose proper design variables to achieve the desired objectives of the linear motor design according to the research results.

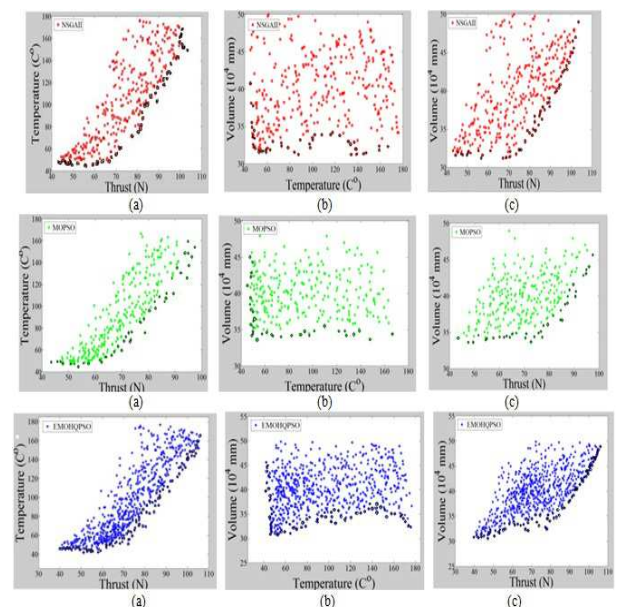


Fig. 4: 2D projections results for (a) NSGA II, (b) MOPSO and (c) EMOHQPSO

Table 3: Results of comparison of RSM-EMOHQPSO and FEA

No.	Design variables							RSM				FEA			
	x_1	x_2	x_3	x_4	x_5	x_6	x_7	Y_P	Y_T	Y_V	D	Y_P	Y_T	Y_V	D
								(N)	(°C)	(cm ³)	(N/cm ³)	(N)	(°C)	(cm ³)	(N/cm ³)
Initial	12.6	4	2.6	0.6	5	3.8	0.4					68.6	99.5	40.1	1.71
1	12.7	4.1	2.2	0.5	5	3.9	0.4	73.2	85.3	39.9	1.83	75.2	94.5	39.9	1.88
2	12.1	4.0	2.5	0.5	5	3.9	0.4	71.9	89.4	38.6	1.86	73.3	97.3	38.6	1.90
3	12.4	4.2	2.2	0.5	5.1	3.7	0.4	71.5	85.9	39.1	1.83	73.9	96.4	39.1	1.89
4	11.7	4.5	2.4	0.5	4.8	4.3	0.4	71.0	83.1	40.0	1.78	72.9	92.9	40.1	1.82
5	11.9	4.1	2.9	0.5	5.2	3.9	0.4	71	85.9	39.4	1.8	75.7	97.7	39.4	1.92
6	12.2	4.1	2.1	0.5	4.8	4.1	0.4	70.8	85.1	39.0	1.82	73.1	94.4	39.0	1.87
7	11.7	4.4	2.7	0.5	4.8	4.0	0.4	70.6	81.8	39.9	1.77	70.2	90.2	39.9	1.76
8	11.3	4.4	2.8	0.5	5.1	4.2	0.4	70.3	83.8	39.3	1.79	75.1	94.2	39.3	1.91
9	13.8	3.4	2.3	0.5	4.8	3.9	0.4	70.3	81.4	40.1	1.75	72.9	92.8	40.0	1.82
10	12.7	3.8	2.6	0.5	5.1	3.9	0.4	70.1	81.6	39.4	1.78	72.5	92.1	39.4	1.84
11	12.9	4.0	2.5	0.5	5.2	3.3	0.4	69.6	78.1	39.5	1.76	69.8	91.1	39.5	1.77
12	12.5	4.2	2.3	0.5	5.3	3.9	0.4	69.5	76.9	39.8	1.75	73.9	90.6	39.8	1.86
13	12.3	4.0	2.2	0.5	5.2	3.4	0.4	69.5	85.6	37.6	1.85	70.1	96.0	37.6	1.86
14	12.6	3.9	2.1	0.5	5.1	3.9	0.4	69.1	79.8	38.7	1.79	73.3	92.5	38.7	1.89

References

[1] K. K. Tan, S. Zhao, Precision Motion Control with a High Gain Disturbance Compensator for Linear Motors, *ISA Transactions*, **43**, 399-412 (2004).

[2] M. J. Chung, D. G. Gweon, Design Optimization and Development of Linear Brushless Permanent Magnet Motor, *International Journal of Control*, **1**, (2003).

[3] A. H. Isfahani, S. V. Zadeh, Design Optimization of a Linear Permanent Magnet Synchronous Motor for Extra Low Force Pulsations, *Journal of Energy Conversion and Management*, **48**, 443-449 (2007).

[4] A. H. Isfahani, B. M. Ebrahimi, H. Lesani, Design Optimization of a Low-Speed Single-Sided Linear Induction Motor for Improved Efficiency and Power Factor, *IEEE Transactions on Magnetics*, **44**, 266-272 (2008).

[5] N. R. Tavana, A. Shoulaie, V. Dinavahi, Analytical Modeling and Design Optimization of Linear Synchronous Motor With Stair-Step-Shaped Magnetic Poles for Electromagnetic Launch Applications, *IEEE Transactions on Plasma Science*, **40**, 519-527 (2012).

[6] K. Ender, O. Ahmet, Modeling of Air Core Permanent-Magnet Linear Motors with a Simplified Nonlinear Magnetic Analysis, *IEEE Transactions on Magnetics*, **47**, 1753-1762 (2011).

[7] P. S. Shin, S. H. Woo, C. S. Koh, An Optimal Design of Large Scale Permanent Magnet Pole Shape Using Adaptive Response Surface Method With Latin Hypercube Sampling Strategy, *IEEE Transactions on Magnetics*, **45**, 214-1217 (2009).

[8] K. Deb, Multi-Objective Optimization Using Evolutionary Algorithms: An Introduction, (2011).

[9] C. Shin, C. Choi, W. Lee, Advance Angle Calculation for Improvement of the Torque-to Current Ratio of Brushless DC Motor Drives, *Energy Procedia*, **14**, (2012).

[10] C. E. Hawkes, T. G. Wilson, R. C. Wong, Magnetic-Field-Intensity and Current-Density Distributions in Transformer Windings, *Power Electronics Specialists Conference, 20th Annual IEEE*, **2**, (1989).

[11] M. Norhisam, N. Mariun, J. I. Syed, N. Mariun, Thrust Density Characteristics of Linear DC Motor, *IEEE PEDS*, **2**, (2005).

[12] S. Neseli, S. Yald, E. Turke, Optimization of Tool Geometry Parameters for Turning Operations Based on The Response Surface Methodology, *Measurement*, **44**, 580-587 (2011).

[13] A. M. Bovada, V. A. BOVDA, V. V. DEREVYANKO, V. A. FINKEL, T. V. SUKHAREVA, Electrical and Magnetic Properties of Nd2Fe14B Magnet in Demagnetized and Magnetized States at Low Temperatures, *Journal of Iron and Steel Research*, **13**, 92-96 (2006).

[14] M. Norhisam, H. Wakiwaka, H. Yajima, K. Tamura, The Maximum Thrust Density of Interior Permanent Magnet Linear Synchronous Motor, *Journal of the Magnetics Society of Japan*, **26**, 661-664 (2002).

[15] S. S. Habib, Study of the Parameters in Electrical Discharge Machining through Response Surface Methodology Approach, *Applied Mathematical Modeling*, **33**, 4397-4407 (2009).

[16] C. P. Lee, M. N. Lo Huang, D-Optimal Designs for Second-Order Response Surface Models with Qualitative Factors, *Journal of Data Science*, **9**, 139-153 (2011).

[17] S. Fazlollahi, P. Mandel, G. Becker, F. Marechal, Methods for Multi-Objective Investment and Operating Optimization of Complex Energy Systems, *Energy*, **45**, 12-22 (2012).

[18] T. Antczak, Penalty Function Methods and a Duality Gap for Inverse Optimization Problems, *Nonlinear Analysis: Theory, Methods and Applications*, **71**, 3322-3332 (2009).

[19] G. Wang, G. Zhao, H. Li, Y. Guan, Multi-Objective Optimization Design of The Heating/Cooling Channels of The Steam-Heating Rapid Thermal Response Mold Using Particle Swarm Optimization, *International Journal of Thermal Sciences*, **50**, 790-802 (2011).

[20] L. Huang, M. Xi, J. Sun, An Improved Quantum-Behaved Particle Swarm Optimization with Binary Encoding, 2010

International Conference on Intelligent System Design and Engineering Application (ISDEA), 1, 243-249 (2010).



Wen-Jong Chen

is an assistant professor in the Department of Industrial Education and Technology at National Changhua University of Education (NCUE), Changhua, Taiwan since 2006. He received his M.S. degree (1994) and Ph.D. (2003) in the Institute of Applied Mechanics and Department of Mechanical Engineering from National Taiwan University, Taipei, Taiwan, respectively. Chen's research areas and interests consist of Control System, Artificial Intelligent and Opto-Mechatronic system integration.



Wen-Cheng Su received the B.S. degree from the Department of Mechanical Engineering of the Oriental Institute of Technology(OIT), Xinbei, Taiwan. He received his M.S. degree from the Department of Industrial Education and Technology at National Changhua

University of Education, Changhua, Taiwan, in (2012). His research areas and interests consist of finite-element analysis in linear motor and Engineering Optimization.



Yin-Liang Yang

is currently a graduate student in the Department of Industrial Education and Technology at National Changhua University of Education (NCUE), Changhua, Taiwan. He received his B.S. degree from the Department of Industrial Education and Technology at National Changhua University of Education, Changhua, Taiwan, in (2012). His research areas and interests consist of CAD/CAM and finite-element analysis in linear motor.